Engineering oxygen nanobubbles for the effective reversal of hypoxia

Muhammad Saad Khan, Jangsun Hwang, Youngmin Seo, Kyusoon Shin, Kyungwoo Lee, Chanhwi Park, Yonghyun Choi, Jong Wook Hong & Jonghoon Choi

Published online: 23 Jul 2018.

Submit your article to this journal ☑

Article views: 367

View related articles ☑

View Crossmark data ☑

Citing articles: 3 View citing articles ☑

Taylor & Francis
Taylor & Francis Group

Check for updates

Engineering oxygen nanobubbles for the effective reversal of hypoxia

Muhammad Saad Khan[a], Jangsun Hwang[a], Youngmin Seo[b], Kyusoon Shin[c], Kyungwoo Lee[a], Chanhwi Park[a], Yonghyun Choi[a], Jong Wook Hong[c,d]* and Jonghoon Choi[a]* [ID]

[a]School of Integrative Engineering, Chung-Ang University, Seoul, Republic of Korea; [b]Center for Biomaterials, Biomedical Research Institute, Korea Institute of Science and Technology, Seoul, Republic of Korea; [c]Department of Nanobiotechnology, Graduate School, Hanyang University, Seoul, Republic of Korea; [d]Department of Bionano Engineering, Hanyang University, Ansan, Republic of Korea

ABSTRACT

Hypoxia, which results from an inadequate supply of oxygen, is a major cause of concern in cancer therapy as it is associated with a reduction in the effectiveness of chemotherapy and radiotherapy in cancer treatment. Overexpression and stabilization of hypoxia-inducible factor 1α (HIF-1α) protein in tumours, due to hypoxia, results in poor prognosis and increased patient mortality. To increase oxygen tension in hypoxic areas, micro- and nanobubbles have been investigated by various researchers. In the present research, lipid-shelled oxygen nanobubbles (ONBs) were synthesized through a sonication method to reverse hypoxic conditions created in a custom-made hypoxic chamber. Release of oxygen gas from ONBs in deoxygenated water was evaluated by measuring dissolved oxygen. Hypoxic conditions were evaluated by performing *in vitro* experiments on MDA-MB231 breast cancer cells through the expression of HIF-1α and the fluorescence of image-iT[TM] hypoxia reagent. The results indicated the degradation of HIF-1α after the introduction of ONBs. We propose that ONBs are successful in reversing hypoxia, downregulating HIF-1α, and improving cellular conditions, leading to further medical applications.

Introduction

Tissue hypoxia is the inadequate supply of oxygen to the tissues due to various reasons and can lead to severe medical complications [1–4]. Normal oxygen pressure varies between tissues; but in most cases, the physiological range for normal tissues lies between 4% and 8% of oxygen level and cellular hypoxia is defined in the range of 1–5% for most tissues [5]. Hypoxia may occur due to reduced cardiac output, reduced haemoglobin concentration, reduced oxygen supply or atypical vasculature of tumour tissue [3,4,6]. Hypoxic tumours are known to be more resistant to chemotherapy and radiotherapy leading to poor prognosis and higher patient mortality [4,6–10]. A relatively small increase in oxygen partial pressure in a hypoxic area can instantaneously increase its radiation sensitization [11]. Chemotherapy usually requires the proliferation of cells for higher cytotoxicity but tumour cells under hypoxia divide slowly, limiting the effectiveness of chemotherapeutic agents [5].

One prominent impact of hypoxic conditions is the expression and stabilization of hypoxia-inducible factor 1α (HIF-1α) protein in tumour cells that affect tumour proliferation, metabolism, apoptosis, vascularization and immune responses, and as a result, HIF-1α is responsible for higher tumour resistance to chemotherapy and radiotherapy [3,4,6,9,12,13]. HIF-1α is sensitive to oxygen and it responds to oxygen deficiency; under hypoxic conditions, HIF-1α is not

hydroxylated, resulting in the stabilization and overexpression of HIF-1α, especially in the case of solid tumours like breast, lung, skin and prostate cancers [4]. Downregulation of HIF-1α may lead to cancer suppression, and thus, various studies have targeted silencing/inhibiting HIF-1α to improve therapeutic efficiency [3,4,6]. Providing adequate oxygen in hypoxic regions would help in the degradation of HIF-1α, and might increase treatment efficacy. Hypoxic conditions are also a major cause of concern in bone tissue engineering and 3D scaffold preparation [14].

To overcome hypoxia and hypoxemia, various methods have been employed to increase *in vitro* oxygen levels. Blood can carry limited oxygen and injecting oxygen gas directly into the blood has the limitation that haemolysis may occur [15]. Inspired oxygen, nitric oxide inhalation, increased red blood cell count, hyperbaric oxygenation, carbogen inhalation, hydrogen peroxide injections, and ozone therapy have been investigated but found ineffective due to their clinical and logistic limitations. There is an urgent requirement for an oxygen source that is cost effective, biocompatible and easy to use [7,10,16–19].

Micro- and nanobubbles are inherently echogenic particles composed of a monolayer shell and a gas core [20]. Traditionally, they have been used as ultrasound contrast agents [11,21–25]. Typically, microbubbles, which are used for diagnostic applications, have sizes ranging between 1 and 10 μm [26]. Uncoated air bubbles dissolve rapidly in the

CONTACT Jonghoon Choi ✉ nanomed@cau.ac.kr ⊞ School of Integrative Engineering, Chung-Ang University, Seoul 06974, Republic of Korea; Jong Wook Hong ✉ jwh@hanyang.ac.kr ⊞ Department of BioNano Engineering, Hanyang University, Ansan 15588, Republic of Korea
*Both authors contributed equally to this work.

bloodstream and a shell coating provides stability for these bubbles and makes them effective for targeted gas/drug delivery [22]. The solubility of gases in fluid is limited and micro- and nanobubbles provide an efficient gas solubility, which helps in synthesizing supersaturated fluids [27]. A variety of shell compositions, higher surface area, higher pay load and biocompatibility makes microbubbles a promising candidate for therapeutic and gas delivery applications [15,28–31]. Recent studies have shown that micro- and nano-bubbles can be used to increase the oxygen partial pressure in tumours through intratumour injections in animal models [10]. However, their limitation is associated with the concentration of microparticles that can be injected without causing adverse effects [19].

Therapeutic applications require reduced size of these bubbles for penetration into the cells. Therefore, nanobubbles have recently gained more attention for therapeutic purposes [22]. Nanobubbles are different from liposomes as liposomes have lipid bilayer shells with an aqueous core and they are less echogenic, whereas nanobubbles have mono-layer shells with a hydrophobic gas core and a hydrophilic shell arrangement [32,33]. Various researchers have used the term nano to indicate particles in the size range 100–800 nm, differentiating these particles from liposomes and microbub-bles [34,35]. Nanobubbles can be separated from microbub-bles by centrifugation and filtration processes. The small size of nanobubbles is suitable for overcoming the problems associated with the size of microbubbles as they can pass through the 380–780 nm thick endothelial gap of the tumour tissue, through a passive target mechanism known as the enhanced permeability and retention effect (EPR). Therefore, they can be effective in mitigating hypoxia [16,27,35].

A variety of shell compositions, including lipids, proteins, polymers or nanoparticles, can be employed to synthesize bubbles. Lipid-based formulations have proven to be safe and lipid-based contrast agents are also commercially available [16,22]. Phospholipids have the characteristic of self-assembly around a gas to form a monolayer, with their hydrophilic heads facing the water and their hydrophobic acyl chains facing the gas; hence, each nanobubble is a dis-crete pocket that can be used for delivery of oxygen gas [25,36]. Due to this characteristic of self-assembly, various techniques can be adopted to synthesize bubbles from lipid shells, including sonication, microfluidic devices and vigorous shaking. Lipid monolayers are highly cohesive, and they have low surface tension. Therefore, they form stable bubbles that have the capability to expand and contract, facilitating gas diffusion across the shell; hence, they can be used for gas delivery applications [25].

Stability is a key factor in the synthesis of micro and nano-bubbles. The cohesiveness of lipid shells depends on the length of the acyl chain used; longer chains will result in higher cohesiveness [16]. 1,2-Distearoyl-sn-glycero-3-phospho-choline (DSPC) has been shown to have higher stability and longer gas retention due to a long acyl chain [29,37]. The presence of an emulsifying polyethyleneglycol (PEG) layer on the bubble shell serves the purpose of reducing electrostatic interaction and reducing capillary retention, improving the stability of bubbles against coalescence [19,38]. Emulsifiers and surfactants help in reducing interfacial tension, thereby reduc-ing Laplace pressure and resulting in stabilized bubbles even at smaller sizes in nanosize range [37,38].

In this paper, we propose the synthesis of oxygen nanobub-bles (ONBs) using a sonication technique to reverse hypoxic conditions. We developed a hypoxia chamber by adapting and modifying the ideas presented by Wang et al. [39] to create hypoxic conditions. We evaluated the hypoxic conditions and reversal of hypoxia through the use of image-iT™ hypoxia reagent and degradation of HIF-1α proteins. This article presents the synthesis technique, characterization and applica-tion of ONBs to reverse cellular hypoxia created in a custom-made hypoxia chamber.

Materials and methods

Materials

DSPC, 1,2-distearoyl-**sn**-glycero-3-phosphoethanolamine-N-[ami-no(polyethyleneglycol)-2000] (ammonium salt) (DSPE-PEG-2000Amine) and 1,2-distearoyl-**sn**-glycero-3-phosphoethanol-amine-N-[biotinyl(polyethyleneglycol)-2000] (ammonium salt) (DSPE-PEG-2000-Biotin) were bought from Avanti Polar Lipids (Alabaster, AL). Image-iT hypoxia reagent and fluorescein-avidin conjugate (FITC-avidin) were purchased from Thermo Fisher Scientific (Waltham, MA). Dulbecco's phosphate-buffered saline (DPBS) and chloroform were purchased from Sigma Aldrich (St. Louis, MO). Anti-HIF-1α antibody (mouse) was purchased from Sigma Aldrich (St. Louis, MO).

Synthesis of oxygen nanobubbles

25.2 mg of DSPC, 8.4 mg of DSPE-PEG-2000-amine and 7.95 mg of DSPE-PEG-2000-biotin were dissolved at the molar ratio of 85:8:7 in chloroform inside a three-neck conical flask. The flask was then placed in a hot air oven to evaporate the chloroform to produce a thin dried lipid film. The dried lipid film was rehydrated by adding 10 mL DPBS to obtain a final concentration of 4.16 mg/mL of lipids and sonicated at 5 °C above lipid transition temperatures, using a bathtub sonica-tor till the entire lipid layer was dissolved in DPBS, forming a milky suspension. This suspension was further sonicated using a tip-sonicator at 190 W in the pulsed mode for 5 min in the presence of an oxygen supply to synthesize the nano-bubbles. A cylinder with 99.995% pure oxygen was used for supplying the oxygen during the sonication process. Micro- and nanosized bubbles produced through this process in three-neck conical flask were collected through careful pipet-ting and transferred into conical tube. Large scale visible bubbles mostly remained stuck to the sides of the flask. The collected suspension was centrifuged at 300×g to separate micro and nanosized bubbles. Microbubbles produced during the process mostly floated in the top layer and were usually discarded after filtration through syringe filter of pore size 1 μm. Fluorescent bubbles were prepared by adding 100 μL of FITC-avidin to 10 mL of the suspension and centrifuging the suspension at 300×g for 10 min. Microbubbles produced during the process mostly floated in the top layer and were

usually discarded. Microsize bubbles were collected for characterization by optical and fluorescence microscopy.

To check the cytotoxicity of the constituent lipids, liposomes were prepared in the same manner without oxygenating the sample.

Characterization of oxygen nanobubbles

Optical and fluorescence microscopy, confocal microscopy, scanning electron microscopy (SEM) (Sigma, Carl Zeiss, Oberkochen, Germany) and transmission electron microscopy (TEM) (LIBRA 120, Carl Zeiss, Oberkochen, Germany) were used for characterizing the bubbles. Microsize bubbles were collected for microscopic imaging, while SEM was performed for both microsize and nanosize bubbles. TEM was used for nanosize imaging.

Samples for confocal microscopy and SEM were made by injecting microbubbles into 5% agarose gel. First, agarose gel was heated up to 100 °C, and then ONBs were added during the cooling-down process when the temperature of the agarose gel was below 50 °C. The agarose gel was left to dry, and then thin layers of the dried gel were cut for imaging purposes. These layers were coated with Pt for SEM imaging.

Samples for TEM were prepared by negative staining using uranyl acetate. First, a copper grid was dipped in nanobubbles, dried, and then washed and negatively stained with 1% uranyl acetate solution. These grids were then dried again and used for TEM imaging at 80 kV.

A nanoparticle tracking analyzer (NTA) (Nanosight NS300, Malvern, PA) was used to determine the particle size distribution and the number of nanobubbles. Samples were diluted at 1:10, 1:100 and 1:1000 to determine the effect of dilution on particle size and particle concentration. Dynamic light scattering (DLS) (Malvern, PA) was also used to analyse the nanobubbles. Samples were diluted at 1:100 for DLS readings. The oxygen concentration was measured by using a dissolved oxygen (DO) meter after injecting micro- and nanobubbles in partially deoxygenated water. Three samples of 30 mL water were taken and deoxygenated to 1.4 mg/L oxygen concentration by purging Argon gas through the samples. One sample was left untreated in normal air, while 3 mL oxygen-saturated DPBS (oxygen saturation 16.9 mg/L) was injected in the second sample, and 3 mL ONBs (oxygen saturation 17.1 mg/mL) was injected in the third sample. Measurements were taken for 360 min until all the solutions reached the equilibrium point. The DO meter has a limitation that it measures only DO and therefore, the increase in oxygen content of deoxygenated water was measured for generating the oxygen release profile. ONB stability tests were performed by storing ONBs for 30 days at 4 °C and counting the number of ONBs with an NTA. To check the diffusion of gas out of ONBs, dilution was carried out and size was measured through NTA for increasing dilution ratios. The same phenomenon of reduction in size was observed after dilution of microbubbles (data not shown).

To determine the number of microbubbles, in the suspension, we poured 4 mL of the suspension without filtration into a 15 mL conical tube, and then carefully extracted each mL volume (1st, 2nd, 3rd and 4th) from the conical tube and placed them into separate tubes. We then took a 10 μL sample from each layer by using pipettes and counted using image J software as described later.

Cytotoxicity tests

Cytotoxicity tests were conducted using MDA-MB-231 breast cancer cells. 1×10^5 cells per well were seeded in a 24-well plate. MDA-MB-231 cells were grown to 80% of the confluence and treated with various concentrations of nanobubbles and liposomes (same lipid constituents) over a period of 24 h. The cell viability percentage was measured using an automated cell counter (Juli-Br, NanoEntek, Seoul, Korea) by staining the cells with 4% trypan blue. Three samples were prepared in each category and three readings were taken for each sample.

Creating and testing hypoxic conditions

A customized hypoxia chamber ($20 \times 15 \times 6$ cm) was designed in our lab for creating hypoxic conditions and reversing cellular hypoxia. The chamber consisted of a transparent glass container with a plastic lid. Two holes were made on top of the lid for purging the chamber with argon gas. The chamber seals were then tested for leakage. The hypoxia chamber was cleaned with 70% ethanol and placed in UV light for 3 h prior to use. Six-well or 24-well cell-culture plates were placed inside the chamber during the hypoxia experiment. Argon gas was purged through the chamber for 20 min to replace the air inside the chamber, which was then sealed for 8 h. Image-iT hypoxia reagent, which is a commercially available reagent, was used for the fluorescence of cells under hypoxia [40]. Ten microlitres (10 μM) of image-iT hypoxia reagent was injected into the media at the start of the experiment. Oxygen concentration inside the chamber was not measured during hypoxia experiments and instead an image-IT hypoxia indicator reagent was used as a hypoxia indicator. Several experiments were carried out to determine the optimal time for creating hypoxia conditions in the hypoxia chamber. It was found that 6–8 h incubation in the hypoxia chamber created desired hypoxia conditions with the majority of cells alive and under oxygen stress. After 6–8 h of incubation in the hypoxia chamber, the cell-plate was taken out of the chamber and the cells were treated with ONBs for 30 min and imaged under a fluorescent microscope at excitation and emission wavelengths of 490 and 610 nm, respectively.

HIF-1α assay

HIF-1α expression was also observed and evaluated as a hypoxia indicator. For fluorescence imaging, MDA-MB-231 cells were seeded on an eight-well glass slide (10,000 cells/well) and kept under hypoxic conditions in the hypoxia chamber for 6 h. Then, half of the samples were treated with ONBs, while the remaining half was left untreated, and the eight-well glass slide was incubated under normal conditions for 3 h. HIF-1α expression was evaluated by using FITC-conjugated

anti-HIF-1α antibody and the expression of HIF-1α was observed using fluorescence microscopy. HIF-1α is expressed in cytoplasm and therefore cells were fixed and permeabilized before introducing the anti-HIF-1α antibody. Cells were also stained with DAPI (4′,6-diamidino-2-phenylindole).

Second, the indirect enzyme-linked immunosorbent assay (ELISA) method was used to determine the expression of HIF-1α using 96-well ELISA plates. The same process of incubating cells in the hypoxia chamber was adopted by placing the 96-well plate in the hypoxia chamber for 6 h, and then treating half of the wells with ONBs for 3 h, while the remaining were left untreated. As a control group, one 96-well plate was kept in normal conditions and treated with the same amount of ONBs. For ELISA, proteins were collected using radioimmuno-precipitation assay (RIPA) as the lysis buffer. The primary antibody was monoclonal anti-HIF-1α antibody from mice, and 2% bovine serum albumin (BSA) was used for blocking nonspecific binding. The secondary antibody was anti-mouse IgG-horseradish peroxidase (IgG-HRP) used at the dilution ratio of 1:2000. Then, 2,2′-azino-bis[3-ethylbenzthiazoline-6-sulfonic acid] (ABTS) was used as a peroxidase substrate and absorbance at 410 nm was used to determine the expression of HIF-1α in hypoxic and normal conditions.

Statistical analysis

GraphPad Prism software was used for statistical analysis and graphical representations of the data (GraphPad, La Jolla, CA). t-Tests were performed on the data and significance was checked. Nonsignificant values have been shown as ns in the results section, while *, **, *** and **** describe p values of less than $<.5, .01, .001$ and $.0001$, respectively.

Image analysis using ImageJ software

The size distribution and the number of microbubbles were counted using ImageJ software from optical microscopy images. For this purpose, microbubbles were collected from various levels of the conical tube after centrifugation at $300 \times g$ and counted using ImageJ. The fluorescence of image-iT hypoxia reagent was also quantified using ImageJ by using the images obtained from fluorescence microscopy.

Results

Figure 1 shows a schematic representation of our experiments. ONBs were synthesized in a three-neck flask using a tip-sonicator while supplying oxygen through the other inlet. The shell of the ONBs consisted of a combination of base phospholipid (DSPC), while PEGylated lipids (DSPE-PEG-2000 amine and biotin) served as surfactants. The molar ratios used for the synthesis of DSPC, DSPE-PEG-2000-amine and DSPE-PEG-2000-biotin were 85:8:7, respectively. The hydrophilic heads of phospholipids were facing outwards towards the DPBS solvent and the hydrophobic tails encircled the oxygen gas, thus forming a monolayer shell. Each nanobubble served as a separate packet of oxygen.

During experiments, the synthesized ONBs were used to reverse hypoxic conditions by adding them to tumour cells, which had been under hypoxic conditions. We hypothesized
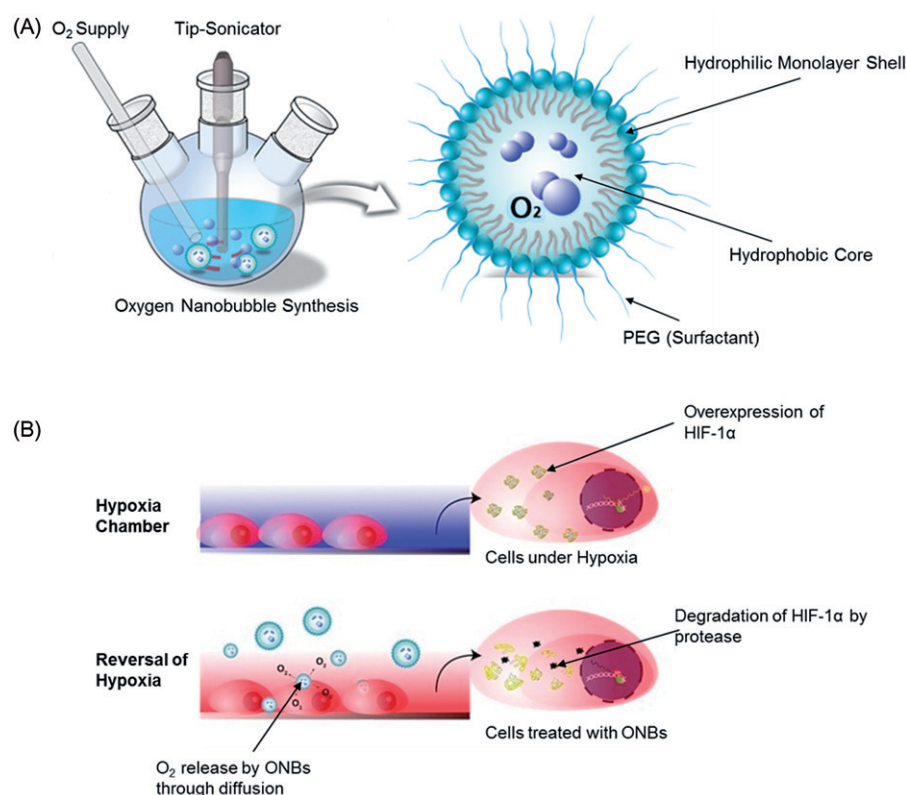

Figure 1. Schematic representation. (A) Schematic diagram of the synthesis of oxygen nanobubbles (ONBs). Lipids are dissolved in DPBS and sonicated in the presence of an oxygen supply. (B) Application of ONBs for the reversal of hypoxia and degradation of HIF-1α expression. It shows the release of oxygen gas from ONBs through a diffusion process that leads to the degradation of HIF-1α.

that treatment with ONBs would help in the degradation of HIF-1α and would improve cell survival, thereby leading to further improvements in the treatment efficacy of chemotherapeutic agents.

Figure 2 demonstrates the characterization of microsized bubbles synthesized during the experiment. Figure 2(A) is the confocal microscopy image demonstrating the poly-disperse size of the microbubbles in agarose gel. The spherical nature of the bubbles can be easily observed. FITC-avidin conjugated with biotin-synthesized fluorescent ONBs is shown in Figure 2(B). For better characterization, larger-sized bubbles were collected and placed on the surface of a glass side. The core–shell nature of the bubbles is evident in the bubbles having a diameter of ∼5 μm or more, indicating that ONBs are most likely to have a similar core–shell nature. Figure 2(C) shows an SEM image of a microbubble with a size of 4.3 μm. The spherical shape is clearly observable in the image. Figure 2(D) shows a size distribution of bubbles measured using ImageJ software. For this, microscopy images were taken and the size was analysed. We found the mean size distribution to be 2.8 μm in the case of microsize particles. Figure 2(E) shows the number of microbubbles collected from various levels of a conical tube. We poured 4 mL of ONB suspension into a 15 mL conical tube, and then carefully extracted each mL volume (1st, 2nd, 3rd and 4th) from the conical tube and placed them into separate tubes. We then took a 10 μL sample from each layer by using pipettes. The top layer contained the highest number of microbubbles (5.5×10^7 microbubbles/mL), and the number of microbubbles decreased as we went down the conical tube to 3.18×10^7 microbubbles/mL, which was a decrease of 42%. This might be attributed to the lower density of microsize

bubbles as they mostly float on the top surface. The average concentration of microbubbles in the solution turned out to be 4.17×10^7 microbubbles/mL, which was ∼10^4 times less than the concentration of nanobubbles in the solution.

The characterization performed for the nanosize bubbles is exhibited in Figure 3. Figure 3(A) is an SEM image showing a nanobubble of the size of ∼500 nm. Figure 3(B) shows TEM imaging of nanobubbles. The shell thickness of the nanobubble is in the range of ∼5–10 nm. The size of the ONBs measured through TEM is in the range of 20–40 nm. Figure 3(C) exhibits data from the NTA analysis showing a mean size of 315 ± 90 nm. The concentration of particles counted was in the range of 4.2×10^{11} nanobubbles/mL. The DLS results, shown in Figure 3(D), also show a similar trend for most nanobubbles in the range of 200–400 nm. The size measured through TEM imaging is much smaller compared to DLS and NTA results and might be due to the vacuuming process carried out during TEM imaging. Owing to the usage of a higher intensity tip-sonicator and a longer duration of sonication, our samples contained more nanobubbles compared to microbubbles, as shown in Figure 3.

Figure 4(A) shows the particle size distribution from NTA data. The 1:100 dilution ratio has a mean size of 350 ± 133 nm. A reduction in the size of the nanobubbles is evident with the increasing dilution ratio as the 1:1000 dilution has a mean size of 267 ± 105 nm, showing that lipid shells allow the diffusion of gas across the particle and therefore their size shrinks. Figure 4(B) reveals the particle count after 30 days and shows that the concentration of particles was reduced to 3.2×10^{11} nanobubbles/mL from an initial mean of 4.22×10^{11} nanobubbles/mL. This indicates a reduction of approximately 30% in the concentration of particles

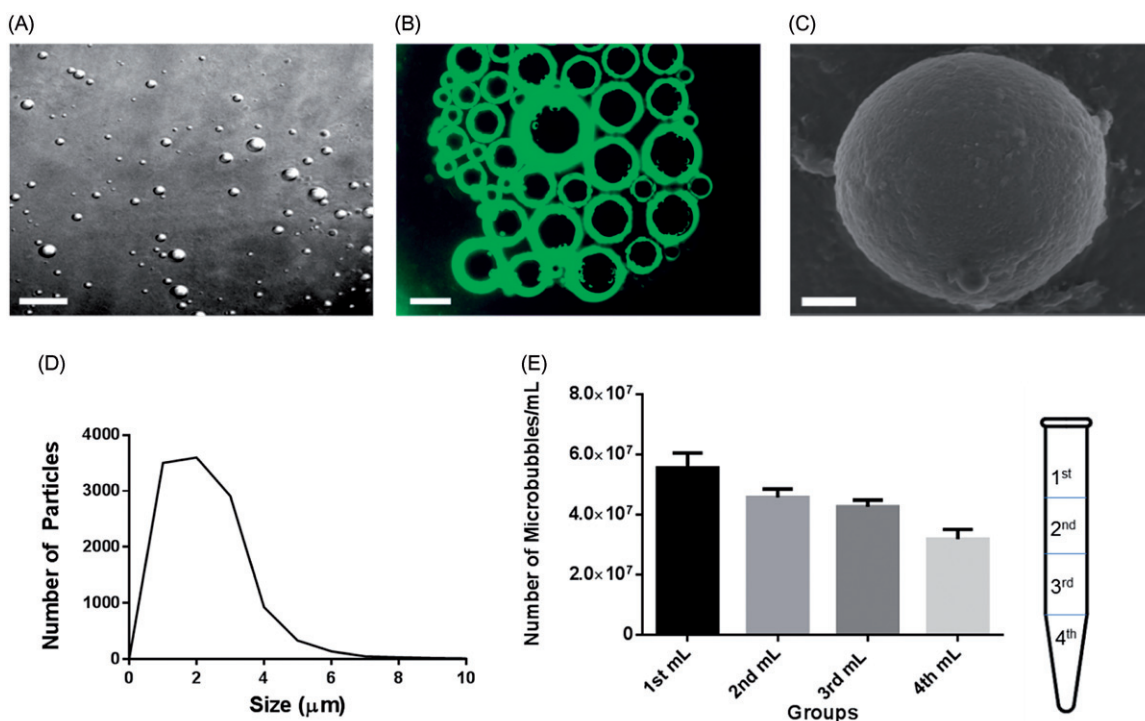**Figure 2.** Characterization of microsize bubbles. (A) Confocal microscopy image of microbubbles, scale bar = 20 μm. (B) Fluorescence microscopy image showing microbubbles, scale bar = 20 μm. (C) SEM image showing a microbubble, scale bar = 1 μm. (D) Size distribution of microbubbles calculated using ImageJ software. (E) Concentration of microbubbles calculated in various sample groups taken from the top to the bottom of a 15 mL conical tube.
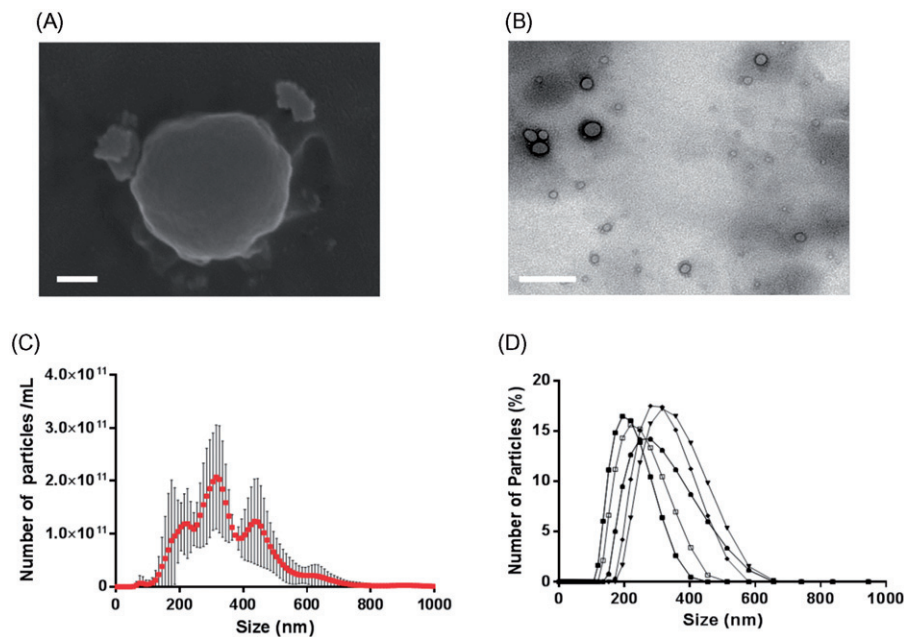
Figure 3. Size distribution of nanobubbles. (A) SEM image of nanobubbles, scale bar = 100 nm. (B) TEM image of nanobubbles, scale bar = 100 nm. (C) NTA results for particle count and size distribution with mean size distribution. (D) DLS results of seven samples of ONBs plotted together to indicate particle size distribution.
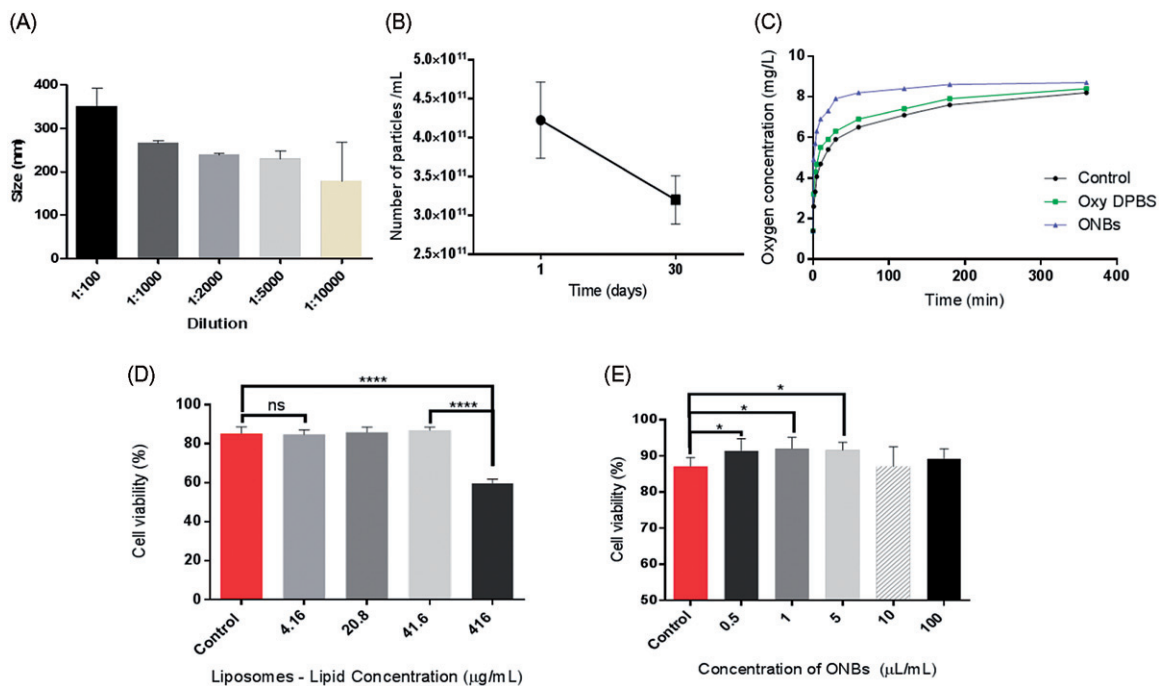

Figure 4. Stability, oxygen delivery and cytotoxicity tests. (A) Size distribution using various dilution ratios of ONBs, obtained through an NTA. (B) Reduction in bubble count after 30 days of storage. (C) Increase in oxygen concentration of deoxygenated water after injection of ONBs and oxygenated DPBS. (D) Cytotoxicity of the lipids used in synthesis of nanobubbles; ns means no significance, ****p values <.0001. (E) Cytotoxicity of ONBs for varying concentrations; *p < .05.

after a period of 30 days. This shows the stability and shelf life of nanobubbles. The size of nanobubbles (data not shown) also remained stable during this time. Figure 4(C) shows the oxygen release profile of ONBs in comparison with oxygenated DPBS and control. Nanobubbles rapidly increased oxygen saturation to ~4.9 mg/mL, as compared to ~3.2 mg/mL of oxygenated DPBS and 2.6 mg/mL of control sample from the starting point of 1.4 mg/mL after 1 min. Most of the nanobubbles released their oxygen in the initial 30 min of injection. The results indicate that ONBs approximately

contained 500 μg/mL more oxygen as compared to oxygenated DPBS, demonstrating that approximately 50% volume of the suspension is oxygen gas. This showed that in a hypoxic environment, the diffusion of the oxygen gas out of bubbles was a rapid phenomenon. Figure 4(D, E) exhibits the cytotoxicity tests conducted for the liposomes at various lipid concentrations and ONBs, respectively. The final concentration of lipids in ONBs was determined to be 4.16 mg/mL and therefore, various concentrations of ONBs shown in Figure 4(E) are comparable to the liposome-lipid concentrations used in

Figure 4(D). Liposomes showed nonsignificant cytotoxicity as compared to a control sample for concentrations up to 41.6 μg/mL. Liposomes at 416 μg/mL (100 μL/mL solution) showed cell viability of ∼60%, nearly 20% less than the control sample. This might be because of a higher concentration of lipids. It is evident that ONBs improved the cell viability by ∼5% compared to the control sample at concentrations of 0.5, 1 and 5 μL/mL. This improvement of cell viability may be attributed to a higher concentration of oxygen available to the cells after the injection of ONBs.

Hypoxic conditions were created in the hypoxia chamber and image-iT hypoxia reagent was used as a hypoxia indicator. Figure 5(A) shows the fluorescence of the image-iT hypoxia reagent control sample when cells were under hypoxic conditions. Bright red fluorescence indicates reduced oxygen levels in the cells. Figure 5(B,C) shows the fluorescence of MDA-MB-231 cells when they were treated with 10% and 20% ONBs solutions, respectively. The reduction in fluorescence of image-iT hypoxia reagent is an indicator of the reversal of hypoxia. Figure 5(D) shows the cells incubated under normal conditions with the same 10 μM image-IT hypoxia reagent. No significant fluorescence could be observed in normal conditions. Figure 5(E) shows a quantification of the fluorescence of image-iT hypoxia reagent using ImageJ software. Control samples showed higher fluorescence (mean fluorescence

intensity ∼25.14) while the samples treated with 10% and 20% ONBs and normal control solutions showed significantly lower fluorescence intensities (7.4% and 2.3%, respectively). Results under normal conditions showed no significance as compared to 20% ONBs. Figure 5(F) shows the cell viability of MDA-MB-231 cells after the hypoxia experiment. The 10% ONB solution shows significantly higher cell survival (>60% cell viability) while the 20% ONB solution does not show a significant difference from the control sample in terms of cell viability (∼40% cell viability). This indicates that the cells were able to survive better when they were treated with an optimal quantity of nanobubbles (10%). Higher amounts of nanobubbles (20%) were able to reverse hypoxia successfully but they reduced cell viability (∼46%), and this might be due to the presence of a higher concentration of lipids. This elaborates upon our previous results that a higher concentration of lipids may reduce cell viability. Higher cell viability (∼60%) due to the 10% ONB solution indicates that the ONBs released a significant amount of oxygen via the diffusion process to reverse hypoxic conditions, and this was crucial for cell survival. Cells cultured under normal conditions showed cell viability of 85.14%. Figure 5(G) shows the top view of the custom-made hypoxia chamber. Hypoxia conditions were successfully created by placing six-well or 24-well plates in this chamber and purging argon gas through the chamber as
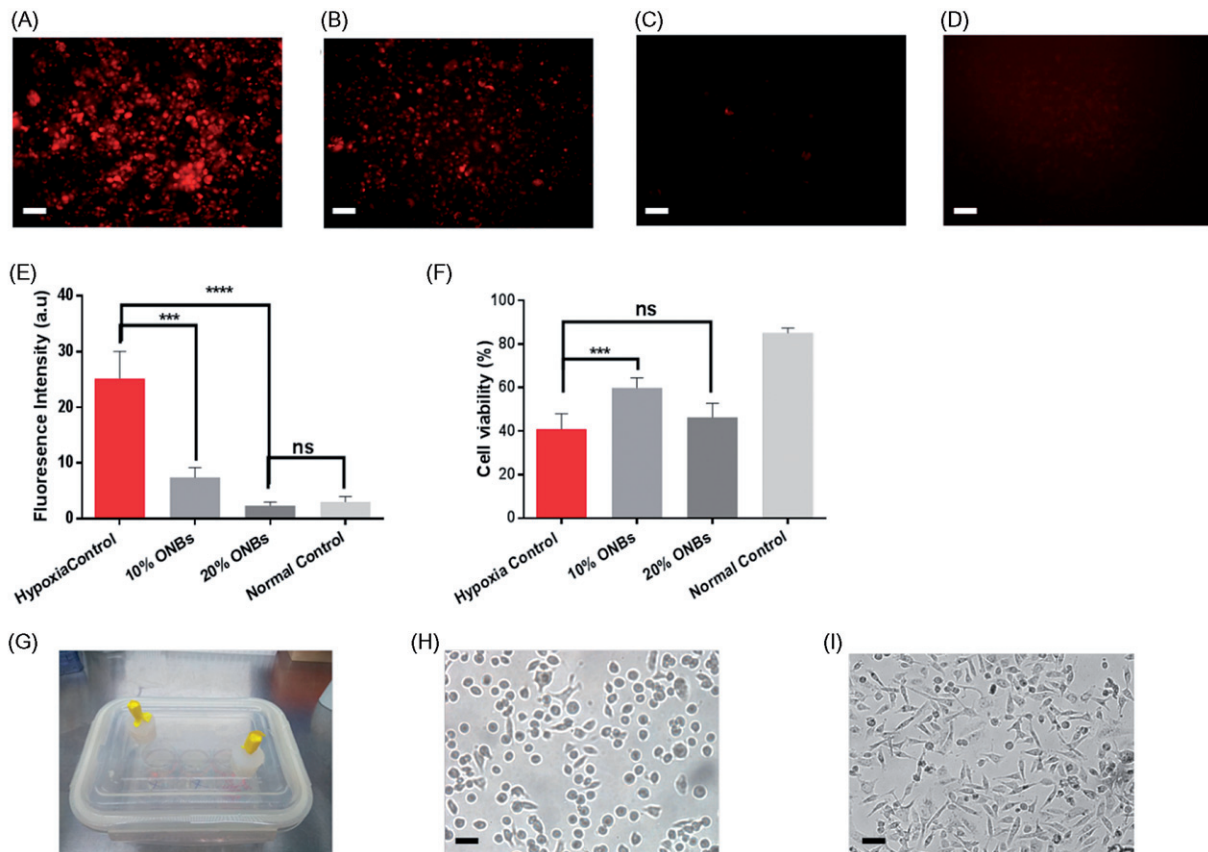

Figure 5. Results of hypoxia experiment. (A) Image-iT fluorescence of MDA-MB-231 cells under hypoxic conditions. Scale bar = 20 μm. (B) Reversal of Hypoxia indicated by reduction in fluorescence when 10% ONB solution was added. (C) Reversal of hypoxia indicated by reduction in fluorescence when 20% ONB solution was added. (D) Fluorescence of image-iT hypoxia reagent under normal incubation conditions as normal control. (E) Fluorescence intensity of image-iT hypoxia reagent compared through ImageJ software in hypoxic conditions, reversal of hypoxic conditions, and normal control; ***$p < .001$, ****$p < .0001$, $n = 4$. (F) Cell viability measured by trypan blue staining in hypoxic conditions, reversal of hypoxic conditions using 10% and 20% ONB solutions, and normal conditions; ***$p < .001$, ns means no significant difference, $n = 3$. (G) Picture of hypoxia chamber used for creating hypoxic conditions. (H) Cell morphology of control sample when MDA-MB-231 cells remained under hypoxia and suffered from cell deaths, scale bar = 20 μm. (I) Cell morphology of cell survival after reversal of hypoxia, scale bar = 20 μm.

described previously. Six to eight hours of incubation were found to be optimal time for hypoxic conditions. Figure 5(H) shows the cell morphology of the hypoxia control sample when cells were not treated with ONBs. The cells were found to be round-shaped and having different morphology. Figure 5(I) shows cell morphology when the cells were treated with 10% ONBs and most of the cells survived after treatment with 10% ONBs.

Figure 6(A) shows a fluorescent image of HIF-1α protein as an indicator of hypoxic conditions. FITC-conjugated anti-HIF-1α antibody and DAPI staining were used for fluorescence imaging. It is clear from the figures that the expression of HIF-1α was reduced when the cells were treated with the 10% ONB solution. Figure 6(B) exhibits the expression of HIF-1α protein evaluated using the indirect ELISA method in comparison with the control sample. Hypoxic conditions show a maximum expression of HIF-1α (mean intensity value 0.26 a.u., $p < .05$) and when the cells were treated with the 10% ONB solution, the expression of HIF-1α reduced (mean intensity 0.20 a.u.). The HIF-1α expression in hypoxic conditions was significantly higher ($p < .01$) when the cells were kept under normal conditions. Cells under normal conditions showed a nonsignificant difference in HIF-1α expression with cells kept under hypoxia and treated with ONBs. Therefore, it can be concluded that ONBs deliver oxygen through diffusion and help in the reversal of hypoxic conditions.

Discussion

In this work, we synthesized lipid-shelled ONBs for oxygen delivery. Phospholipid shells in combination with PEGylated lipid surfactants help in the reduction of bubble size to the nanometre range. They are stable, biocompatible and capable of providing the facility to attach functional groups to the shell of the bubble. DSPC has been used as a base lipid and has been reported to be more stable than some other phosphocholines and allows gas permeability [19]. ONBs were synthesized in the presence of a continuous oxygen supply so that the phospholipids self-assembled around the hydrophobic gas, forming a hydrophilic monolayer shell. We used biotin and amine as functional groups in the

phospholipid shells. The biotin functionality was tested using fluorescence FITC-avidin dye, which successfully conjugated to biotin to make the fluorescent bubble shells shown in the results. This affinity can be further used to add various drugs or nanoparticles to the shells of ONBs.

Optical and fluorescence microscopy were successfully employed to observe and count microbubbles. In particular, microbubbles larger than 5 μm demonstrated clear shell core compositions in fluorescent images. Confocal microscopy images and SEM images taken using agarose gel also showed the spherical shell-surface of microbubbles, while TEM images revealed the core–shell composition of nanobubbles.

An NTA and DLS were able to determine the size range and stability of ONBs and the results from both devices showed similarity with mean sizes in the range of 200–400 nm. The size of ONBs can be controlled by adjusting the parameters of sonication and the composition of lipids. We were able to synthesize a higher concentration of ONBs in the range of 4.2×10^{11} nanobubbles/mL than previously reported in the literature (1×10^9 bubbles/mL) [8] by using a higher concentration of constituent lipids and increasing the time duration of sonication. Our samples included microsize bubbles in the range of 4×10^7 microbubbles/mL, which is approximately 10^4 times less than the concentration of nanobubbles. These microbubbles can be filtered out, thus limiting the size of bubbles in the nano range, which offers higher therapeutic advantages owing to the EPR [16].

The liposome formulation of the same constituents without oxygenation was also used to test the impact of constituent lipids on the cell viability. Results showed that a concentration of 416 μg/mL lipids reduced cell viability by 20–30%. This can be attributed to a higher concentration of lipids. ONBs having concentration of less than 10% media volume were beneficial for cell viability during hypoxia experiments as they improved cell viability by ∼20% compared to the control sample. ONBs in lower concentrations (less than 1%) improved cell viability in normal conditions by ∼5% compared to the control sample. This shows that improved oxygenation through ONBs can be used for improving cell viability.
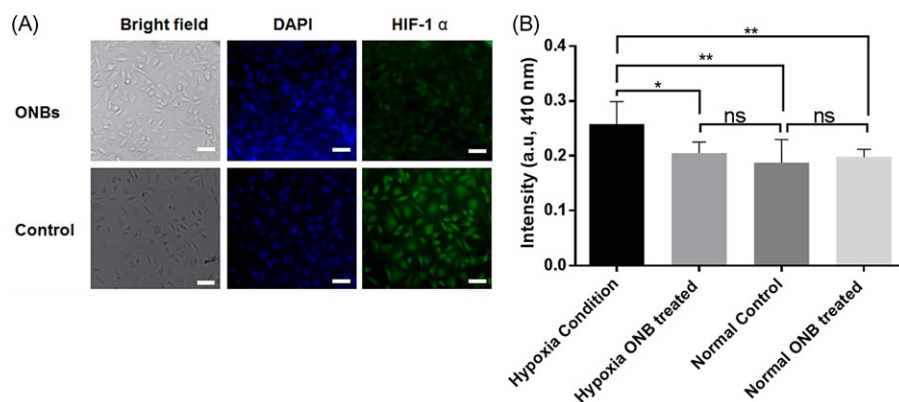

Figure 6. HIF-1α expression assay. (A) Comparison of HIF-1α expression in control and after the reversal of hypoxic conditions. FITC-conjugated anti-HIF-1α antibodies were used along with DAPI staining of MDA-MB-231 cells. The reduced expression of anti-HIF-1α is clearly observable in the fluorescent image, indicating successful degradation of HIF-1α protein due to ONBs. Scale bars = 20 μm. (B) HIF-1α expression evaluated through the indirect ELISA method. The hypoxia control is the untreated sample in hypoxic conditions. Hypoxia bubble means the samples in the hypoxia chamber treated with ONBs. Normal control is an untreated sample in normal conditions. Normal bubble means the samples treated with ONBs in normal conditions; *$p < .05$, **$p < .01$, ns means no significance, $n = 3$.

We used the ONBs to release oxygen via a diffusion mechanism as phospholipids are permeable to gas. Due to the limitation of the DO sensor to detect the oxygen inside the ONB core, the experiment was designed to deliver oxygen to deoxygenated water. The release of oxygen from ONBs was compared to the oxygenated DPBS and control sample. Dissolved oxygen concentration prior to the experiment of ONBs and oxygenated DPBS was similar (17.1 mg/mL and 16.9 mg/mL, respectively). ONBs released approximately 500 μg/mL more oxygen as compared to oxygenated DPBS, demonstrating the successful synthesis of ONBs with oxygen gas as part of their core. This provides evidence that ONBs can be used to supply more oxygen as compared to oxygen-saturated DPBS.

We were able to create hypoxic conditions in a repeatable manner in our low-cost custom-made hypoxia chamber. Overexpression of HIF-1α protein and fluorescence of image-iT hypoxia reagent showed that our hypoxia chamber was able to create the desired hypoxic conditions. Incubation of 6–8 h in the hypoxia chamber, after purging it with argon for 20 min, was enough to observe fluorescence of image-iT hypoxia reagent. The cell viability was approximately 40% in the control sample in the hypoxia experiment, while it increased to 60% when 10% ONBs were used to reverse hypoxia. However, 20% ONBs showed no significant difference in cell viability compared to the control sample. This indicated that a concentration of ONBs 10% or less is better for cell viability and the reversal of hypoxia.

The overexpression and stabilization of HIF-1α has been associated with the higher survival of tumours and therefore several researchers have targeted silencing/inhibiting HIF-1α for better cancer treatment. Our results indicated that HIF-1α expression was reduced in the presence of ONBs and that ONBs can be used for suppressing HIF-1α.

We believe that this model can be repeated in tumours and that the diffusion mechanism can be sufficiently employed to reverse hypoxic conditions in tumours. This may eliminate the requirement of using ultrasound in combination with bubbles, as ONBs can penetrate the tumours using the EPR effect [37].

Conclusions

A synthesis technique for ONBs is presented in this paper. ONBs were successfully employed to reverse hypoxic conditions created in a custom-made hypoxia chamber, with a reduction in the expression of HIF-1α, indicating that they were able to achieve the reversal of hypoxic conditions. ONBs can be conjugated with drugs/biomolecules as evaluated through fluorescent ONBs.

Disclosure statement

No potential conflict of interest was reported by the authors.

ORCID

Jonghoon Choi (iD) http://orcid.org/0000-0003-3554-7033

References

[1] Cavalli R, Bisazza A, Giustetto P, et al. Preparation and characterization of dextran nanobubbles for oxygen delivery. Int J Pharm. 2009;381:160–165.

[2] Magnetto C, Prato M, Khadjavi A, et al. Ultrasound-activated decafluoropentane-cored and chitosan-shelled nanodroplets for oxygen delivery to hypoxic cutaneous tissues. RSC Adv. 2014;4:38433–38441.

[3] Ziello JE, Jovin IS, Huang Y. Hypoxia-inducible factor (HIF)-1 regulatory pathway and its potential for therapeutic intervention in malignancy and ischemia. Yale J Biol Med. 2007;80:51.

[4] Wigerup C, Påhlman S, Bexell D. Therapeutic targeting of hypoxia and hypoxia-inducible factors in cancer. Pharmacol Ther. 2016;164:152–169.

[5] Razorenova OV, Giaccia AJ. Hypoxia, gene expression, and metastasis. The tumor microenvironment. New York (NY): Springer; 2010. p. 43–58.

[6] Rapisarda A, Melillo G. Combination strategies targeting hypoxia inducible factor 1 (HIF-1) for cancer therapy. The tumor microenvironment. New York (NY): Springer; 2010. p. 3–21.

[7] Kwan JJ, Kaya M, Borden MA, Dayton PA. Theranostic oxygen delivery using ultrasound and microbubbles. 2012;2(12):1174.

[8] McEwan C, Owen J, Stride E, et al. Oxygen carrying microbubbles for enhanced sonodynamic therapy of hypoxic tumours. J Control Release. 2015;203:51–56.

[9] Melillo G. Inhibiting hypoxia-inducible factor 1 for cancer therapy. Mol Cancer Res. 2006;4:601–605.

[10] Owen J, McEwan C, Nesbitt H, et al. Reducing tumour hypoxia via oral administration of oxygen nanobubbles. PLoS One. 2016;11:e0168088.

[11] Eisenbrey JR, Albala L, Kramer MR, et al. Development of an ultrasound sensitive oxygen carrier for oxygen delivery to hypoxic tissue. Int J Pharm. 2015;478:361–367.

[12] Zhao W, Hu X, Duan J, et al. Oxygen release from nanobubbles adsorbed on hydrophobic particles. Chem Phys Lett. 2014;608:224–228.

[13] Li F, Mei H, Gao Y, et al. Co-delivery of oxygen and erlotinib by aptamer-modified liposomal complexes to reverse hypoxia-induced drug resistance in lung cancer. Biomaterials. 2017;145:56–71.

[14] Malda J, Klein TJ, Upton Z. The roles of hypoxia in the in vitro engineering of tissues. Tissue Eng. 2007;13:2153–2162.

[15] Kheir JN, Polizzotti BD, Thomson LM, et al. Bulk manufacture of concentrated oxygen gas-filled microparticles for intravenous oxygen delivery. Adv Healthc Mater. 2013;2:1131–1141.

[16] Fix SM, Borden MA, Dayton PA. Therapeutic gas delivery via microbubbles and liposomes. J Control Release. 2015;209:139–149.

[17] Legband ND, Feshitan JA, Borden MA, et al. Evaluation of peritoneal microbubble oxygenation therapy in a rabbit model of hypoxemia. IEEE Trans Biomed Eng. 2015;62:1376–1382.

[18] Black KJ, Lock AT, Thomson LM, et al. Hemodynamic effects of lipid-based oxygen microbubbles via rapid intravenous injection in rodents. Pharm Res. 2017;34:2156–2162.

[19] Feshitan JA, Legband ND, Borden MA, et al. Systemic oxygen delivery by peritoneal perfusion of oxygen microbubbles. Biomaterials. 2014;35:2600–2606.

[20]   Cavalli R, Bisazza A, Lembo D. Micro- and nanobubbles: a versatile non-viral platform for gene delivery. Int J Pharm. 2013;456:437–445.

[21]   Hernot S, Klibanov AL. Microbubbles in ultrasound-triggered drug and gene delivery. Adv Drug Deliv Rev. 2008;60:1153–1166.

[22]   Unger EC, Porter T, Culp W, et al. Therapeutic applications of lipid-coated microbubbles. Adv Drug Deliv Rev. 2004;56:1291–1314.

[23]   Geers B, Lentacker I, Sanders NN, et al. Self-assembled liposome-loaded microbubbles: the missing link for safe and efficient ultrasound triggered drug-delivery. J Control Release. 2011;152:249–256.

[24]   McDannold N, Zhang Y, Vykhodtseva N. The effects of oxygen on ultrasound-induced blood–brain barrier disruption in mice. Ultrasound Med Biol. 2017;43:469–475.

[25]   Sirsi S, Borden M. Microbubble compositions, properties and bio-medical applications. Bubble Sci Eng Technol. 2009;1:3–17.

[26]   Liu Y, Miyoshi H, Nakamura M. Encapsulated ultrasound micro-bubbles: therapeutic application in drug/gene delivery. J Control Release. 2006;114:89–99.

[27]   Matsuki N, Takuji I, Shingo I, Naoki S, Yoshihito U, Takami Y. Oxygen supersaturated fluid using fine micro/nanobubbles. Int J Nanomed. 2014;9:4495.

[28]   Yoon YI, Kwon Y-S, Cho H-S, et al. Ultrasound-mediated gene and drug delivery using a microbubble-liposome particle system. Theranostics. 2014;4:1133.

[29]   Swanson EJ, Mohan V, Kheir J, et al. Phospholipid-stabilized microbubble foam for injectable oxygen delivery. Langmuir. 2010;26:15726–15729.

[30]   Swanson EJ, Borden MA. Injectable oxygen delivery based on protein-shelled microbubbles. Nano Life. 2010;01:215–218.

[31]   Gerber F, Waton G, Krafft MP, et al. Long lived microbubbles for oxygen delivery. Artif Cells Blood Subst Biotechnol. 2007;35:119–124.

[32]   Koshiyama K, Wada S. Collapse of a lipid-coated nanobubble and subsequent liposome formation. Sci Rep. 2016;6:28164.

[33]   Pitt WG, Husseini GA, Staples BJ. Ultrasonic drug delivery—a general review. Expert Opin Drug Deliv. 2004;1:37–56.

[34]   Bhandari P, Wang X, Irudayaraj J. Oxygen nanobubble tracking by light scattering in single cells and tissues. ACS Nano. 2017;11:2682–2688.

[35]   Bhandari PN, Cui Y, Elzey BD, et al. Oxygen nanobubbles revert hypoxia by methylation programming. Sci Rep. 2017;7:9268.

[36]   Kheir JN, Scharp LA, Borden MA, et al. Oxygen gas-filled micropar-ticles provide intravenous oxygen delivery. Sci Transl Med. 2012;4:140ra88.

[37]   Cavalli R, Soster M, Argenziano M. Nanobubbles: a promising efficient tool for therapeutic delivery. Ther Deliv. 2016;7:117–138.

[38]   Lee M, Lee EY, Lee D, et al. Stabilization and fabrication of microbubbles: applications for medical purposes and functional materials. Soft Matter. 2015;11:2067–2079.

[39]   Wang R, Jin F, Zhong H. A novel experimental hypoxia chamber for cell culture. Am J Cancer Res. 2014;4:53.

[40]   Zhang S, Hosaka M, Yoshihara T, et al. Phosphorescent light-emit-ting iridium complexes serve as a hypoxia-sensing probe for tumor imaging in living animals. Cancer Res. 2010;70:4490–4498.